Desalination and Water Treatment
www.deswater.com

doi: 10.5004/dwt.2022.28269

252 (2022) 300–318
March

A solution of taste and odor problem with activated carbon adsorption in drinking water: detailed kinetics and isotherms

Alper Alver[a,*], Emine Baştürk[a], Levent Altaş[b], Mustafa Işık[b]

[a]*Department of Environmental Protection and Technologies, Technical Sciences Vocational School, Aksaray University, Aksaray, Turkey, Tel. +903822883630; Fax: +903822883525; email: alperalver@gmail.com (A. Alver) ORCID: 0000-0003-2734-8544, Tel. +903822883601; Fax: +903822883525; email: eminebasturk@hotmail.com (E. Baştürk) ORCID: 0000-0002-1628-5026*
[b]*Department of Environmental Engineering, Engineering Faculty, Aksaray University, Aksaray, Turkey, Tel. +903822883591; Fax: +903822883525; email: laltas@yahoo.com (L. Altaş) ORCID: 0000-0002-9738-560X, Tel. +903822883610; Fax: +903822883525; email: mustafaisik55@hotmail.com (M. Işık) ORCID: 0000-0002-8440-2546*

Received 26 September 2021; Accepted 3 February 2022

ABSTRACT

In this study, 2-methylisoborneol (2-MIB) and geosmin (GSM) adsorption pathways on steam-activated wood-originated powder activated carbon were investigated. Firstly, EN 12903 analysis was carried out, giving information about the activation, origin, and suitability of usability as an adsorbent in drinking water treatment plants of activated carbon, and it was found that it was activated by steam, was of wood origin, and suitable for the basic requirements for the adsorption of 2-MIB and GSM. A series of experiments including contact time, the concentration of metabolites, initial pH of the solution, and dosage of activated carbon were performed on raw surface water samples. Many kinetic and isotherm models known in the literature have been applied to explain the 2-MIB and GSM adsorption on powdered activated carbon (PAC). As a striking feature of the isotherm models, it was concluded that the multilayer physical and/or chemical adsorptions of 2-MIB (R^2_{BET} = 0.636) and GSM (R^2_{BET} = 0.777) occurs on the macro and mesopores of PAC, the adsorption capacity of PAC is higher for 2-MIB (k_F = 0.146, q_e = 0.9904) than for GSM (k_F = 0.023, q_e = 0.9252), and the adsorption of GSM (R_L = 0.970) and 2-MIB (R_L = 0.951) on PAC are reversible. Among the kinetic models, the pseudo-second-order model was found to be the most successful in describing the adsorption of 2-MIB and GSM on the PAC. According to the pseudo-second-order kinetic model, the chemical or physical adsorption situation is not in equilibrium. Therefore, the intraparticle diffusion model applied to find the adsorption mechanism shows that 2-MIB and GSM are physically adsorbed on the external surface of the PAC in the first 16 min, and diffusion from macropores to meso and micropores occurs during the next 74 min. More time is needed for the adsorption to reach equilibrium.

Keywords: Methylisoborneol; Geosmin; Taste; Odor; Activated carbon; Adsorption; Kinetics; Isotherms

1. Introduction

Nitrogen and phosphorus elements that are abundant in the aquatic environment cause excessive proliferation of photosynthetic species such as algae and aquatic plants. This rapid and overgrowth results in eutrophication and eventually leads to impaired water quality. The eutrophication importantly exacerbates water quality and diminishes the biodiversity of the aquatic ecosystem [1]. As a result, the problem of taste and smell is quite common in waters supplied from eutrophic water sources. The two most important substances that cause taste, earthly odor, and mildew

* Corresponding author.

in drinking water are geosmin (1,10-dimethyl-trans-9-decalol; $C_{12}H_{22}O$) and 2-methylisoborneol (2-methylisoborneol; $C_{11}H_{20}O$) which are produced by the metabolism and degradation of cyanobacteria, and which is present probably in eutrophication processes [2]. Algal and bacterial growth arise from these non-toxic compounds. In the water basin, these compounds may be inclined, especially in severe conditions of algal blooms [3–5]. As humans perceive a major drawback of these two substances at even very low concentrations (4–20 ng L^{-1}) [6], they are among the chief complaints in the water sector, especially in places where water is supplied from eutrophic water sources [7].

Geosmin (GSM) is produced by the gram-positive bacteria Streptomyces and various cyanobacteria and released when these microorganisms die [8,9]. Communities whose water supplies depend on surface water can periodically experience episodes of unpleasant-tasting water when a sharp drop in the population of these bacteria releases GSM into the local water supply. Under acidic conditions, GSM decomposes into odorless substances [10].

The primary source and production of 2-methylisoborneol (2-MIB) is the metabolism and biodegradation of cyanobacteria such as *Pseudanabaena* sp., *Oscillatoria* sp., and *Planktothrix* sp. in warmer climates [6,11]. The occurrence of taste and odor compounds are related to both inside and outside algae cells that are classified as intracellular and extracellular. The extracellular removal of taste and odor compounds was inefficient by conventional treatment methods [12]. In contrast, the intracellular removal rate was higher. However, this situation brings more questions, such as achieving intracellular removal, and cell damage occurring, and the release of these compounds on the water body [13]. Hence, it could be hypothesized that these compounds were not easily removed from the water body. Three main points where taste and odor problems may occur in the journey of drinking water from a water source to a consumer tap are surface water source, treatment plant, and distribution network [14]. The taste and odor problem occurring in the water resources is tried to be minimized by basin protection measures such as the addition of algicide. In water treatment plants, alternative methods such as adding powdered activated carbon (PAC) to existing units or integrating advanced oxidation processes are applied. The source of the taste and odor problem in distribution networks is tried to be determined [15].

Classical water treatment processes, mostly coagulation–flocculation, filtration, and disinfection, are sufficient for turbidity and pathogen removal but do not guarantee removal of micropollutants that cause taste and odor [6,16]. Although ozonation, membrane filtration, or combined processes called advanced water treatment processes can be proposed for effective removal of these substances causing taste and odor, powdered activated carbon adsorption is often the method of choice as considering flexibility, low cost, and sponge-like properties [17–19]. At the date of publication of the European Standard, powdered activated carbon was not listed as a dangerous substance [20]. The product is stable but hygroscopic. It can be stored for an unlimited time if kept dry and away from volatile materials. Generally, PAC is added to the first stage of the water treatment plant, as this application allows for the longest contact time possible before other treatment chemicals are added. Several factors control the PAC sorption characteristics. These factors incorporate PAC properties (e.g., pore structure, surface area, raw material, bulk density, and particle size), the presence of natural organic matter in the raw water, and water treatment processes [21].

Determining the appropriate PAC dosage to be added to the raw water in taste and odor removal is very important in terms of efficiency and operating cost. Many kinetic and isotherm studies have been carried out in the literature to design adsorption systems for the removal of target and similar pollutants. Although many researchers suggest that the model, they use to design their adsorption systems is the most suitable, there is no prominent kinetic and isotherm model in the design of 2-MIB and GSM removal. Therefore, firstly, the objective of this project was to determine a procedure for optimal PAC dosing (isotherm) and equilibrium time (kinetics) estimation to remove geosmin and 2-MIB for real surface water used as a resource for a drinking water treatment plant. An accurate mathematical description of the equilibrium isotherms and kinetics is essential to the effective design of 2-MIB and GSM sorption on PAC. Therefore, the second objective was to use several error analysis methods to determine the best-fitting isotherm and kinetics equation.

2. Materials and methods

2.1. Water resource and characterization

The water resource examined in this study is a soil body fill type dam and has a water volume of approximately 10 hm^3, 70% of it is used for drinking water supply as well as for recreational purposes. The region and the water resource were kept confidential in order not to be shared with 3rd party people and institutions. The water quality parameters were analyzed in the samples taken from the water intake structure of the dam, to determine the effects of water inlets and outlets and waterfront activities on the water quality. In addition to 2-MIB and GSM parameters, test methods for other parameters analyzed for raw water characterization are given in Table 4.

2.2. Analytical procedure

The 2-MIB and GSM concentrations were determined immediately by using liquid/liquid extraction combined with gas chromatography/mass spectrometry (GC/MS), according to Shimadzu [22]. Analytical equipment and conditions of the gas chromatography method and obtained analytical details are given in Table S1 for measurements of 2-MIB and GSM, respectively.

The methods of the parameters analyzed for activated carbon characterization are specified in Table 5 under Sub-Title 3.2. Additionally, scanning electron microscopy (SEM) images of some activated carbons obtained before and after pollutant adsorption were determined using the Hitachi SU1510, Hitachi High Technologies, USA, electron device at 500, 1,000, 2,000, and 5,000 magnification rates, and the structures were examined. The optical column and sample were kept in a vacuum, such as 10^{-4} Pa. In experiments, the secondary electron detector was used, and the voltage was selected as 20 kV.

2.3. Experimental procedure

Coconut-originated powdered activated carbon was preferred to be used as an adsorbent in experiments. The solutions used for calibration and spike are freshly prepared and validated for each set from GSM (CAS: 16423-19-1), and 2-MIB (CAS: 2371-42-8) certified reference materials supplied by Sigma-Aldrich (Germany).

In the batch system, the orbital shaker operated at 22°C ± 2°C room temperature and 75 rpm rotation speed throughout all the sorption tests. A different concentration between 50 and 500 mg PAC L^{-1} was introduced into 250 mL solutions in a 500 mL volumetric flask containing a target concentration of 2-MIB and GSM spiked to raw water: the initial pH was adjusted with concentrated and/or diluted H_2SO_4 (CAS: 7664-93-9) and NaOH (CAS: 1310-73-2). Then, the experiment was started by adding the desired amount of sorbent to the flasks containing GSM or 2-MIB. The samples were withdrawn from the flask at predetermined intervals up to 90 min, which was assumed as the maximum time for real drinking water treatment plants (WTP). Samples taken at the time intervals determined during the experiment were centrifuged and filtered with a 0.45 μm membrane to remove the solid sorbents; 2-MIB and GSM concentrations remaining in the supernatant were determined by GC/MS analysis of extracts obtained after liquid–liquid extraction with a 2.5-fold enrichment rate.

2.4. Theory and models

2.4.1. Adsorption kinetics and isotherm models

Sorption kinetics is a curve that shows the rate of release of a sorbate from a water environment to solid-phase (sorbate) under controlled conditions such as concentrations of sorbate, the dosage of sorbent, initial pH, temperature, etc. [23]. Various kinetic models have been applied to investigate the sorption time, optimum sorbent dosage, and sorption mechanism for 2-MIB and GSM removal.

Adsorption isotherms are used to describe how sorbates interact with adsorbent materials, so modeling adsorption isotherm data is essential for predicting and comparing adsorption performance: such as the calculation of the capacities of adsorbents [24].

The sorption occurs in three stages as macro transport, meso/micro transport, and sorption on the inner surface of the sorbent [25]. Macro transport involves the movement by advection and diffusion towards the liquid–solid interface from the liquid phase of the sorbate. Micro transport involves diffusion towards the sorption points in the micro and sub-micro pores of the substance to be adsorbed. Sorption mechanisms are used to determine the time, speed, type, and condition of these stages. Table S2 gives the used models with non-linear and linear form, plot, and slope and intercept terms in this study.

2.4.2. Error functions

Linear regression analysis, adsorption kinetics, and isotherm tests, which have been applied frequently for the analysis of experimental data, are among the most obvious and applicable tools. These tools are used to quantify the distribution of adsorbents and to define the optimal relationship invalidating the consistency of adsorption models and the theoretical assumptions of adsorption models. In a comparison of models, in some cases, the correlation coefficient may not be sufficient alone in the model coefficients determined by the linearization technique. It is necessary to evaluate statistically which model of the experiment fits best. There are many methods related to this evaluation. The most common evaluation technique is to calculate and determine the error functions of the model result calculated for each measurement result. It can be assumed that the model fits well with the experimental results when the average relative error is less than 5%.

The error structure of the experimental data shows the comparison of the theoretical data obtained after the conversion of the adsorption isotherms into linearized forms with the experimental data. This is inevitable against this background, as it provides a mathematically rigorous method to determine adsorption parameters using the form of isotherm equations of linearized regression analysis. As a result, the error functions commonly used in the literature to find the most suitable isotherm and kinetic model for experimental data are given in Table S3. You can find more detailed information about error functions in Ayawei et al. [26] study.

3. Results and discussion

3.1. Water characterization

The growth curve of algae causing 2-MIB and GSM formation generally consists of a lag phase, rapid (logarithmic) growth phase, stagnation phase, and death phase. Therefore, the concentrations of these metabolites vary in parallel with these stages. The lag or delay phase is the ideal timeframe to detect the beginning of the taste and odor problem. If it is late, the situation can quickly get out of control during the logarithmic growth phase. Taylor et al. [27] observed rapid increases in the GSM concentration in lake water from 10 to 300–400 ng L^{-1} in a few days unless preventions were applied. Considering the shortness of this period, the importance of establishing an early warning mechanism becomes evident once again. For this reason, it is essential to monitor algae growth and eutrophication-related water quality parameters in the water supply.

Water quality classes of the parameters specified in Table 1 were identified, and the current status of the water source with 2-MIB and GSM problems was revealed. Since the central question of the study is the optimization of removal by PAC adsorption in the rapid mixing unit, the correlation with water quality parameters will be given in more detail in later studies.

Although it can be said that the quality of the water source, whose analysis results are given in Table 1, varies between Class I–III throughout the year, usually Class I according to the Turkish Surface Water Quality Management Regulation, there is a taste and odor problem [28]. Especially in the summer season, algae growth occurred in conditions rich in nutrients where the temperature is 20°C and above. These algae growths can contribute to the formation of products that cause taste

Table 1
Characteristics of raw water

Parameters*	Methods	Average ± Standard deviation
Geosmin (ng L^{-1})	Agilent 5991-1031	24.9 ± 18.7
2-Methylisoborneol (ng L^{-1})	Agilent 5991-1031	58.2 ± 30.2
t (°C)	SM 2550 B	12.2 ± 6.30
Dissolved oxygen	SM 4500-O C	9.43 ± 1.66
pH	SM 4500-H+ B	8.51 ± 0.39
Conductivity (mS cm^{-1})	SM 2510 B	0.26 ± 0.03
Total dissolved solids	SM 2540 C	143 ± 19.9
Cl_2^-	SM 4110 B	4.36 ± 1.23
NH_4–N	SM 4500-NH_3 B, C	0.03 ± 0.01
NO_3–N	SM 4110 B	0.08 ± 0.03
SO_4	SM 4110 B	10.1 ± 3.27
Total phosphorus	EPA 200.7	0.06 ± 0.04
Biochemical oxygen demand	SM 5210 D	1.60 ± 0.28
Chemical oxygen demand	SM 5220 D	12.9 ± 9.09
Ca	EPA 200.7	38.4 ± 5.28
Mg	EPA 200.7	2.59 ± 0.80
CO_3	SM 2320 B	1.83 ± 1.75
HCO_3	SM 2320 B	132 ± 14.6
As	EPA 200.7	0.008 ± 0.005

*All parameters not specified in units are given in mg L^{-1}. n = 4 for 2-MIB and GSM analysis and n = 12 for other analyses.

and odor problems. The odor detection limit for 2-MIB and GSM is between 9 and 13 ng L^{-1}, so the target to be determined must remain below this range [29]. Although neither the US EPA nor the WHO has declared the limit value related to these compounds, the criterion is stated to be the acceptable odor for consumers [30]. However, the total odor number limit value is <3.

Phosphorus is one of the key nutrients that play an important role in the growth of cyanobacteria in eutrophic lakes. Therefore, the increase in phosphorus concentration is a precursor to the taste and odor problem. Similar to Işık [31] study, the trophic level in dams was determined as mesotrophic and eutrophic according to this parameter, it is known that blue-green algae are dominant and algal foam and macrophyte problems occur at these levels (Trophical Level Index = 47.370–70.589). In the study by Sabater et al. [32], it was found that ideal conditions for mass growth of blue-green algae were found in the water source (~0.4 mg L^{-1}), where the high phosphorus level was observed when nitrogen was limiting. Just like in this study, Watson [33] and Downing et al. [34] stated that the medium phosphorus level caused a cyanobacterial explosion in the period corresponding to late summer and autumn, and found that the phosphorus level in the range of 30–70 μg L^{-1} was the ideal range for cyanobacterial growth.

It has been stated that the presence of living groups (cyanobacteria, other algae, actinomycetes, and fungi), which may be possible producers of 2-MIB and GSM in network systems, indicates the deficiencies in the water distribution system or purification system. WHO has limited cyanotoxin concentrations to 1 μg L^{-1} for safe water resources. To prevent taste and odor problems on the surface, drinking water resources, especially the sources transporting nutrients to stagnant waters should be subject to continuous control, or living groups' growth, should be restricted. In cases where taste and odor formation cannot be prevented at the source, information about the applicability of activated carbon adsorption, which is one of the typical taste and odor removal methods, to drinking water treatment plants is given in the continuation of the study. First, the physicochemical characterization of the activated carbon used in the study was examined.

3.2. Characterization of powdered activated carbon

Activated carbon is used in the treatment of pollutants in liquid or gaseous media, in addition to its also used in many different sectors such as food, defense, and metal industries. In the treatment processes, the physicochemical properties of the adsorbent are key in explaining the mechanisms that will play an active role in the adsorption of the target pollutant and in predicting the removal percent. Also, water-soluble substances on the surface of the adsorbent should not be toxic to water. For this purpose, physical and chemical characterization of the commercial PAC was conducted using a lot of methods in the standard of "BS EN 12903:2009, products used for the treatment of water intended for human consumption – powdered activated carbon" and other referenced methods [35]. Results and conformity of assessment of the PAC are shown in Table 2.

Commercial carbons can be prepared from various raw materials, including wood, lignite, coal, bone, oil residues, and coconut shells [36–38]. The raw material is usually activated in an atmosphere consisting of CO_2, CO, O_2, H_2O

Table 2
Determination of activated carbon origin

Parameter		Method	Limit	Result
Appearance		–	Black powder	Black powder
pH_{PZC}		pH Drift	–	8.81
BET, $m^2\ g^{-1}$		EN 12902	–	908
Apparent density, kg m^{-3}		EN 12902	–	358 ± 24
Particle-size distribution, μm	d10	Mie Theory	–	2.750
	d50		–	13.07
	d90		–	51.13
	d95		150	62.76
Bulk density, g cm^{-3}		ASTM D 8176-18	0.350 ± 0.035	0.377 ± 0.001
Ash content, %		ASTM D 2866-11	15.00	14.1 ± 0.2
Water content, %		ASTM D 2867-99	5.000	1.9 ± 0.1
Water-extractable substances	Arsenic (As), μg g^{-1}	TS EN ISO 17294-2	10.00	0.037
	Cadmium (Cd), μg g^{-1}		0.500	<0.005
	Chromium (Cr), μg g^{-1}		5.000	<0.010
	Mercury (Hg), μg g^{-1}		0.300	<0.001
	Nickel (Ni), μg g^{-1}		15.00	<0.010
	Lead (Pb), μg g^{-1}		5.000	<0.005
	Antimony (Sb), μg g^{-1}		3.000	<0.030
	Selenium (Se), μg g^{-1}		3.000	0.029
	Cyanide (CN), μg L^{-1}	EPA 9010 C-9014	5.000	<0.050
Content of zinc (Zn), μg L^{-1}		TS EN ISO 17294-2	2.000	<0.010
İodine number, mg g^{-1}		ASTM D-4607-94	>600	1,086.574 ± 108.657
Methylene blue index, mg g^{-1}		ASTM C1777-14	–	286.8 ± 28.68
PAH_{Total}, μg g^{-1}	Acenaphthene	ISO 17993	<0.200	<0.0001 <0.0024
	Acenaphthylene			<0.0001
	Anthracene			<0.0001
	Benzo(a)anthracene			0.0003
	Benzo(a)pyrene			<0.0001
	Benzo(b)fluoranthene			<0.0001
	Benzo(g,h,i)perylene			<0.0001
	Benzo(k)fluoranthene			<0.0001
	Chrysene			0.0003
	Dibenzo(a,h)anthracene			<0.0001
	Fluoranthene			<0.0001
	Fluorene			<0.0001
	Indeno(1,2,3-cd)pyrene			<0.0001
	Naphthalene			<0.0001
	Phenanthrene			<0.0001
	Pyrene			0.0005

vapor, air, or other selected gases, at temperatures between 300°C and 1,100°C, followed by air or water cooling. Due to the impure nature of the raw materials used in the production of commercial carbons and the concentration and temperature gradients that develop within the carbon beds during activation, surfaces that are very heterogeneous or difficult to characterize can be formed [39]. If the carbon surfaces are activated at temperatures lower than 500°C, it is considered to be acidic, and those activated at higher temperatures are considered to be "basic", so the pH_{PZC} value of the PAC has been controlled and found to be 8.81 [40]. This data is accepted as an indication that carbon is activated at temperatures higher than 500°C.

Adsorption is a phenomenon of surface, so the presence of porous structures is important. The main physical properties of the adsorbent material (activated carbon) are associated with the type of its pore structure. Internal pore volumes, the most crucial adsorptive feature of activated carbon, are limited by the surface area. The total pore volume of the ideal structure of active carbon is around 0.2–1.0 $cm^3\ g^{-1}$. Although the surface area is in the range of 400–1,000 $m^2\ g^{-1}$, this value can be exceeded in

special-purpose productions. Pore sizes vary in the range from 0.3 to thousands of nanometers [41]. The total surface area associated with the small geometrical regions of the granules or particles of the substance indicates the presence of a large internal surface, which can only be provided by small capillaries. In this study, iodine number, which is a frequently used parameter in water treatment applications, was examined both as an indicator of the micropores and, as a parameter that shows the activation level of activated carbon, was determined as 1,086 mg g^{-1}. This PAC with a high iodine number has high micropores and is therefore particularly suitable for adsorption of micropollutants such as 2-MIB and GSM.

Another test method that represents the micropores (>15 angstroms) and small mesopores (<100 angstroms) of PAC is the methylene blue index test. Although there are different test methods for the methylene blue index in many different units, none of them are standardized test methods by ASTM or EN. Just like the iodine number, there is no correct relationship between methylene blue index and organic matter with large and small molecules removal efficiency of PAC. If it is desired to estimate how much organic matter can be adsorbed on the activated carbon, the Molasses Number test representing macropores and mesopores in PAC would be a better choice.

The water-extractable substances and the total polyaromatic hydrocarbons data in Table 2 generally show that PAC is a suitable product used for the treatment of water intended for human consumption.

It has been stated in previous studies that the adsorption capacity of activated carbons is related to the small and regular pore system [42]. In this study, the structure and dimensions of the pores were tried to be determined by SEM images given in Fig. 1.

The image taken by electron microscopy in the "Macropore" range, which shows the highly developed porosity of activated carbon, is given in Fig. 1. As seen in Fig. 1, activated carbon particles have different pores: micropores (<1 nm), mesopores (1–25 nm), and macropores (>25 nm) [43]. The structures that give adsorption capacity are micro and mesopores. Macro pores allow rapid entry of target contaminants into mesopores and micropores (into the particle) where actual adsorption occurs. Since the PAC particle sizes are small, macropores are generally absent, but this does not create a disadvantage for the adsorption of micropollutants. All pores are formed during the activation process. Activation is simply to develop pores in nonporous raw material with the activation processes. There are two types of activation processes. These are "steam activation" and "chemical activation", respectively, for historical use. These two processes give mainly different pore structures.

In steam-activated carbons such as our use, all of the carbonized raw materials consist of minimal graphite-like

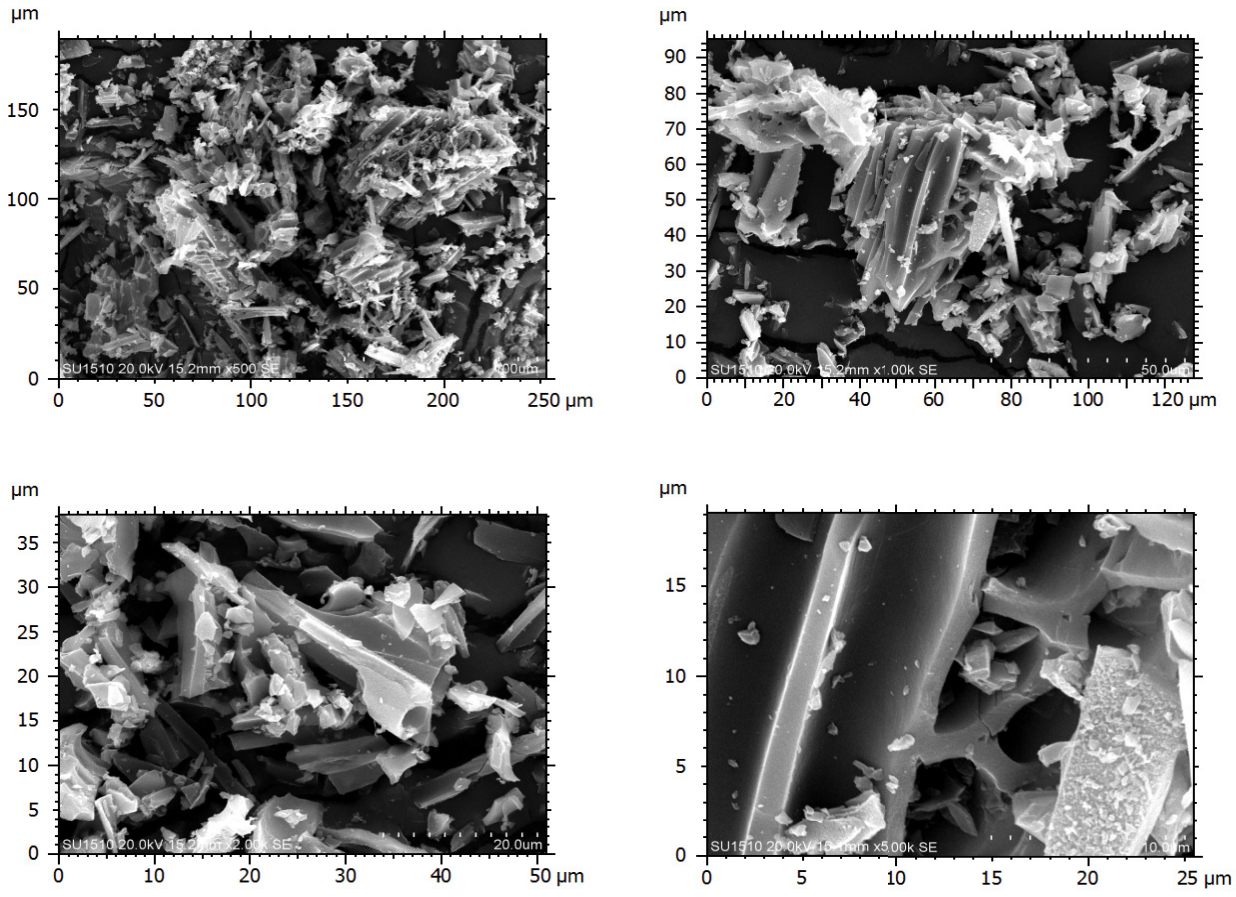

Fig. 1. SEM images of the coconut originated activated carbons.

surfaces called "basal surfaces". Basal surfaces are mostly composed of aromatic carbon atoms, with some surface functional groups containing other atoms at the ends [39]. Basal surfaces are flat or twisted, 0.35 nm thick, and several nanometers wide and long. In carbonized matter, many basal surfaces can most often be stacked. Numerous adjacent surfaces in the same direction form a graphite-like heap. In other places, the direction of the surfaces is completely random [44]. In the steam activation process, the carbonized substance is reacted with steam at a temperature of about 1,000°C. Under these conditions, some of the carbon atoms go by gassing. Due to many factors, different basal surfaces in the carbonized substance show various activities during this gassing reaction. As a result, some surfaces are removed while others remain. Thus, a very porous structure is formed. As a result of the production method, micropores are generally slit-shaped. Micropore walls are wide straight edges adjacent to basal surfaces. Activation gradually expands the micropores to the mesopores.

Consequently, when the distribution of the pore sizes of this activated carbon is examined, due to the presence of both micro and mesopores, it has been found to have a character that allows multi-purpose use. It has a very large surface area, excellent pore volume, low water-extractable substances content, and chemical stability that make it ideal for liquid phase applications where macropore and mesopore sites are important. For example, coconut shell-based carbons, which have a fully microporous structure, are only suitable for removing low molecular weight substances. In contrast, lignite-based activated carbons with larger mesopores are more effective in removing high molecular weight substances (e.g., colored structures, humic substances). Because the presence of substances with higher molecular weight mostly obstructs the inlet of the micropores and prevents adsorption performance. However, chemically activated carbons compared to steam-activated carbons provide less hydrophobic and more negatively charged pore surface [45]. In the later parts of the study, the adsorption rates and mechanisms of the 2-MIB and GSM components on the steam-activated carbon surface were examined, and the unknown ones were tried to be understood by their adsorption.

3.3. Factors affecting adsorption

All adsorption experiments were carried out by spiking GSM and MIB components on real water samples. The main purpose is to determine how adsorption removal efficiencies are affected in the presence of other competitive pollutants in addition to GSM and MIB metabolites in the aquatic environment. Thus, it is aimed to achieve more feasible results in reality.

3.3.1. Contact time and concentration of metabolites

Fig. 2a shows the relationship between the adsorption rate on PAC and time at four initial concentrations of 2-MIB and GSM. The removal efficiency and adsorption capacity of compounds by PAC were increased with an increase in contact time and then reached a maximum value. The first step of the adsorption process took 0–15 min to reach the relative sorption equilibrium named fast adsorption. This performance was due to the binding process between sorbates and the active sites of the adsorbent, and functional groups on the PAC adsorbent were fully and efficiently completed. After this step, in the slow adsorption process, the absorption rate of the sorbates was controlled by the rate of the sorbates transported from the water to the surface of the PAC particles. After 15 min of contact time, the adsorption rate decreased and gradually stabilized with the increase of time. This case was caused to the binding process between sorbates and PAC active sites, and functional groups of PAC were steadily saturated. As a result, adsorption rates of 2-MIB and GSM were controlled by the compounds transported from exterior to interior pore sites of the PAC particles [46].

Fig. 2b shows the relationship between the adsorption capacity and percentage of PAC at four initial concentrations of 2-MIB and GSM. Adsorption percentage and the uptake of 2-MIB and GSM are dependent on the initial concentration of the sorbates. Not only do the rates of sorption decrease but also the equilibrium adsorption capacities (q_e) increase with increasing both sorbate concentrations. This is because there are enough active areas at a lower concentration that the sorbate can easily cover. However, at higher concentrations, active sorption zones are not sufficiently available to occupy the sorbate [46].

3.3.2. Initial pH

The effect of water pH on adsorption of 2-MIB and GSM from the water was studied under identical conditions (acidic, neutral, and basic conditions). The change of pH value in the adsorption system could lead to the transformation of chemical characteristics on the surface of activated carbon and the form of the adsorbate. Thus it plays an important role in adsorption [47]. The data are shown in Fig. 2c, which represents that the adsorption behavior of both compounds was similar from pH 3.02 to 10.03. As can be seen, the alkaline condition was favorable for the adsorption of 2-MIB and GSM on PAC. For both compounds, a significant decrease in adsorption capacity was observed in the acidic conditions (i.e., a reduction of about 25%–30% removal at pH 3.02). The selected pH for further adsorption experiments was pH 7.05 because the adsorption capacity was very similar to the maximum (~0.95 mg g^{-1}), and real conditions of PAC addition in WTP, so that using basic pH does not have any significant advantage. Interestingly, since no studies investigating the pH effect in PAC adsorption studies on 2-MIB and GSM have been found, a comparison of these results with the literature has not been made. However, it was found that increased pH increased the adsorption efficiency in studies related to PAC adsorption of a similar organic methylene blue dye [46,48].

Generally, PAC has the acid functional groups are carboxylic, lactonic, and phenolic, and the basic functional groups include oxygen-containing species such as ketonic, pyronic, chromenic, and p-electron systems of carbon basal planes [49]. Lower adsorption of 2-MIB and GSM at acidic pH might be due to the presence of excess H^+ ions

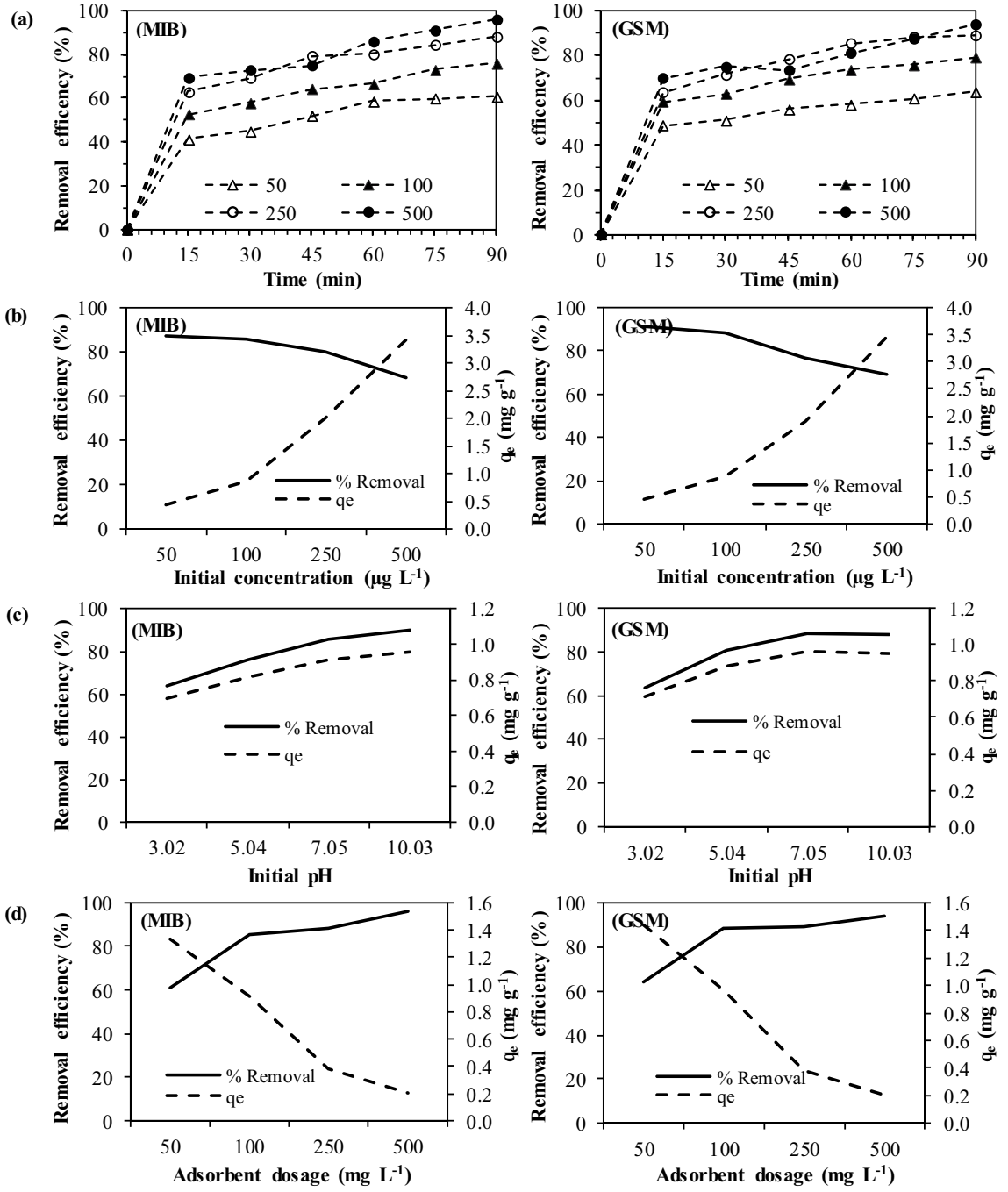

Fig. 2. Removal efficiency and q_e values of 2-MIB and GSM vs. (a) time ([2-MIB, GSM] = 100 µg L^{-1}, pH = 7.05), (b) sorbate concentration ([PAC] = 100 mg L^{-1}, pH = 7.05, t = 90 min), (c) initial pHs ([GSM, 2-MIB] = 100 µg L^{-1}, [PAC] = 100 mg L^{-1}, t = 90 min), and (d) sorbent dosage ([2-MIB, GSM] = 100 µg L^{-1}, pH = 7.05, t = 90 min).

competing with a positive site of compounds functional groups for the available adsorption sites.

3.3.3. Dosage of activated carbon

The adsorbent dose is an important factor that affects the adsorption performance. The percentage removal resorcinol by adsorption onto activated carbon adsorbent was studied by varying the adsorbent dose in the range from 50 to 500 mg L^{-1}, with 100 µg L^{-1} of 2-MIB and GSM spiked raw water, at agitation time of 200 rpm, at a fixed pH = 7.05 and a temperature of 20°C.

The effect of initial PAC concentration on removal efficiency of 2-MIB and GSM is presented in Fig. 2d, which indicated a rapid increase in sorption with increasing PAC concentrations. Removal efficiencies were about 96% and 94% at 500 mg L^{-1} of PAC for 2-MIB and GSM, respectively. Higher doses are not expected to be higher sorption, and

high doses are not suitable for practical application. As expected from the general mechanism of sorption, since the concentration of PAC increased, the sorption rate of compounds gradually increased due to the increases in the number of sorbents pores and adsorption sites. The sorption would tend to an equilibrium when the mass of sorbent reached a certain concentration. The results show that about 100 mg L^{-1} PAC concentrations are required for the effective removal of 100 μg L^{-1} taste and odor compounds.

3.4. Theory and models

3.4.1. Kinetics

Firstly, a kinetic study was done out to investigate the removal of 2-MIB and GSM with PAC, and then an isotherm study was carried out. Determining the sorption rate and identifying the potential rate-controlling step is essential for practical sorption and isotherm study. The experimental data were utilized with the zero-order, first-order, second-order, pseudo-first-order, pseudo-second-order. The special characteristics of each model were evaluated based on the rate coefficient, the coefficient of determination, and some error coefficients, which are seen in Table 3.

Sorption is accepted to occur by two general mechanisms, physical and chemical. While in physical sorption, it occurs on the surface of sorbent with weak forces such as van der Waals for attraction, and in chemical sorption, it is formed by strong bonds where electron exchange occurs between a sorbent and sorbate into all sites. Sorption kinetics of a sorbent depends on the surface and/or pore areas and the present active sites on these areas and the affinity of sorbates to sorbents [50,51].

The pseudo-first-order model is the empirical kinetic equation for one-site occupancy sorption, which simulates rapid sorption due to the absence of sorbent–sorbate interaction. The pseudo-second-order model involves all the potential sorption procedures, such as external film diffusion, surface sorption, and intraparticle diffusion [52,53].

Accordingly, it can be concluded that the adsorption process is based on chemical reactions involving electron exchange between the sorbent surface and the sorbate, according to the pseudo-second-order kinetic parameters [54]. In pseudo-second-order kinetic, the chemical or physical adsorption situation was not in balance, so the mechanism should be investigated. We also researched the adsorption mechanism of the 2-MIB and GSM on the PAC.

3.4.2. Isotherms

It is crucial to carry out the most correlation for the curves between pollutant concentrations of water and sorbent to optimize the design of the sorption process. Numerous isotherm models were used to find the relationship between the amount of adsorbed material and the residue in solution to evaluate the equilibrium characteristics of the sorption processes onto PAC for 2-MIB and GSM. Moreover, Freundlich, Langmuir, Temkin, Dubinin–Radushkevich, Brunauer–Emmett–Teller, Harkins–Jura, Halsey, Redlich–Peterson, Sips, and Toth isotherm models that are categorized as two and three-parameter isotherm, were investigated. Results of 2-MIB and GSM sorption isotherms are shown in Table 4 for all studied models.

As can be seen in Table 4, the R^2 values are either the most important factor or the average relative error values

Table 3
Kinetic parameters for different models (optimum experimental conditions)

Kinetics	Zero-order	First-order	Second-order	Pseudo-first-order	Pseudo-second-order
2-MIB					
Parameters	k_0 = 0.3362	k_1 = 0.0131	k_2 = 0.0005	k_1 = 0.0324	k_2 = 0.0947
	C_0 = 44.5137	C_0 = 50.6131	C_0 = 76.8836	q_e = 0.4884	q_e = 0.9904
R^2	0.9878	0.9878	0.9694	0.8862	0.9905
SSE	0.0005	0.0008	0.0064	0.0047	0.0086
SAE	0.0516	0.0531	0.1354	0.1437	0.1830
ARE	1.0745	1.1601	3.1332	3.1692	4.1628
HYBRID	0.0312	0.0751	1.3539	1.2973	1.1389
MPSD	0.9224	0.9306	0.9579	0.9575	0.9562
χ^2	0.0007	0.0010	0.0094	0.0064	0.0123
GSM					
Parameters	k = 0.2936	k = 0.0091	k = 0.0003	k = 0.0323	k = 0.1176
	C_0 = 47.6722	C_0 = 50.6677	C_0 = 57.5	q_e = 0.4006	q_e = 0.9252
R^2	0.9705	0.9877	0.9896	0.9789	0.9965
SSE	0.0010	0.0005	0.0008	0.0022	0.0057
SAE	0.0714	0.0440	0.0501	0.0885	0.1369
ARE	1.5801	0.9937	1.2118	2.0839	3.3130
HYBRID	0.0623	0.0823	0.1061	0.9011	0.9031
MPSD	0.9288	0.9314	0.9338	0.9540	0.9540
χ^2	0.0014	0.0007	0.0012	0.0031	0.0087

Table 4
Isotherm parameters for different models

Isotherms	Freundlich	Langmuir	Temkin	Dubinin–Radushkevich	Brunauer–Emmett–Teller	Harkins–Jura	Halsey	Redlich–Peterson	Sips	Toth
2-MIB										
Parameters	k_F = 0.146 1/n = 0.636	k_L = 0.007 R_L = 0.951 q_{max} = 7.071	k_T = 0.084 b_T = 1.642	k_D = 0.008 q_S = 1.011 E = 7.714	C_{BET} = 0.942 q_S = 1.274 Cs = 19.675	A_{HJ} = 1.072 B_{HJ} = 2.301	k_H = 0.049 n_H = 1.573	k_R = 0.051 A_R = 0.007 β = 0.997	k_S = 0.018 n = 0.649	k_T = 0.007 n_T = 1.282
R^2	0.954	0.922	0.934	0.760	0.636	0.859	0.954	0.895	0.877	0.957
SSE	0.900	0.420	0.573	21.433	5.763	5.784	0.900	0.442	0.689	2.987
SAE	1.494	1.049	1.251	7.219	3.756	3.777	1.494	0.977	1.471	2.875
ARE	10.829	10.966	17.094	50.075	34.455	26.823	10.829	10.055	17.645	24.915
HYBRID	1.730	0.307	0.391	94.834	19.594	46.212	1.730	6.746	6.411	99.66
MPSD	0.960	0.944	0.946	1.000	0.984	0.992	0.960	0.973	0.973	1.000
χ^2	0.234	0.153	0.299	5.219	1.428	1.422	0.234	0.169	0.337	0.865
GSM										
Parameters	k_F = 0.023 1/n = 1.093	k_L = 0.001 R_L = 0.970 q_{max} = 35.334	k_T = 0.039 b_T = 0.792	k_D = 0.003 q_S = 1.005 E = 12.768	C_{BET} = 0.840 q_S = 0.798 Cs = 30.045	A_{HJ} = 0.724 B_{HJ} = 2.151	k_H = 0.032 n_H = 0.915	k_R = 0.056 A_R = 1.737 β = 0.240	k_S = 0.012 n = 0.556	k_T = 0.006 n_T = 1.968
R^2	0.997	0.546	0.953	0.842	0.777	0.816	0.997	0.659	0.980	0.992
SSE	0.137	0.198	0.836	0.137	145.762	16.924	0.137	0.126	1.798	3.812
SAE	0.569	0.678	1.808	0.568	14.071	5.915	0.569	0.553	1.767	2.787
ARE	3.403	4.356	24.147	4.398	83.319	33.768	3.403	3.397	11.408	15.866
HYBRID	0.171	0.021	8.520	4.316	157.337	57.185	0.171	0.954	17.880	2.682
MPSD	0.938	0.919	0.976	0.969	1.005	0.994	0.938	0.955	0.983	0.965
χ^2	0.029	0.043	0.465	0.036	23.115	2.983	0.029	0.027	0.312	0.264

are crucial to determine the best fitting isotherm. The average relative errors (ARE) values should be less than 5% as defined by the section error functions; due to the results, none of them is less than 5% for 2-MIB, and the Langmuir, Freundlich, Halsey, and Redlich–Peterson models are less than 5% for GSM. Together these results provide crucial insights into not only R^2 but also ARE values are essential to determine the fitting models. Thought as both pollutants, the Langmuir, Freundlich, Halsey, and Redlich–Peterson models were well suited.

According to the results, the R^2 values of Freundlich and Langmuir isotherms for 2-MIB are close to each other. Whether a similar relationship between Freundlich and Langmuir occurred, the Redlich–Peterson isotherm model should be used that reported in the literature. This model is widely used as a compromise between Langmuir and Freundlich systems. The value of β is between 0 and 1. When the value of β is near or equal to 1, the above equation is fitted to the Langmuir isotherm. The β coefficient of the Redlich–Peterson model for GSM adsorption was found to be 0.2403 and it can be said that the isotherm is suitable for the Freundlich model [55]. The β value is 0.9927 for 2-MIB, so the isotherm is suited to the Langmuir model. This situation was also paralleled to R^2 values.

Freundlich equation is an experimental expression that includes the heterogeneity of the surface and the exponential distribution and energies of the active sites [56]. The k_F (L μg^{-1}) in the Freundlich isotherm indicates the relative adsorption capacity constant of the sorbent, and $1/n$ indicates the intensity of the adsorption. According to the $1/n$ value for GSM, it can be said that adsorption for 2-MIB shows proper development and chemically developed, while adsorption behaves physically. It can also be said that PAC has a higher capacity to adsorb 2-MIB than GSM.

The admissibility of the adsorption system is related to the irreversibility of that system, and this relationship has been examined with the Langmuir isotherm. The approach of the R_L value obtained from the Langmuir isotherm to zero indicates a completely ideal irreversible situation [57]. R_L values are in the range of $0 < R_L < 1$, and it has been shown that the adsorption of 2-MIB and GSM on the PAC are reversible in the studied range. k_L is Langmuir constant related to adsorption capacity (μg mg^{-1}), which can be correlated with the variation of the suitable area and porosity of the adsorbent that is more suitable for 2-MIB sorption than GSM.

The Temkin isotherm is another two-parameter isotherm model established upon the theoretical hypothesis that the decline of the heat was linear with the amount of sorption due to adsorbate with sorbent interactions [58]. The bad fitness indicates that the temperature of sorption is independent of the sorption amount, and the sorption may not only be chemical [53].

The Dubinin–Radushkevich isotherm model is a semi-experimental equation in which adsorption follows a pore-filling mechanism [59], and its distinctive feature is the fact that it depends on temperature; therefore, neither GSM nor 2-MIB sorption on PAC can be said to develop depending on temperature.

The Brunauer–Emmett–Teller (BET) isotherm is related to the adsorption of pollutants on materials surface by van der Waals forces that are created by a film of the adsorbate [60]. The adsorption may be physical by van der Waals forces or chemical by a chemical reaction between material and adsorbate. The temperature, sorbent material, pressure, and surface area are the most important parameters that affect adsorption at BET isotherm that is similar to the Langmuir theory that consists of monolayer adsorption [61]. Due to the low R^2 values, for 2-MIB and GSM, the multilayer physical adsorption and/or chemical adsorption occurred.

Harkins–Jura isotherm model assumes the possibility of multilayer adsorption on the surface of sorbent having heterogeneous pore distribution [62] and showed a better fit to the adsorption data like as Freundlich isotherm for GSM.

The fitting of experimental data to the Halsey isotherm model attests to the heterosporous nature of the sorbent. Similar to Song et al. [59] study, the Halsey isotherm fits the experimental data well due to the high correlation coefficient (R^2), which may be attributed to the heterogeneous distribution of activating sites and multilayer adsorption on PAC.

Sips isotherm is a combination of the Langmuir and Freundlich isotherms, and the parameters of this isotherm model are pH, temperature, and concentration [63]. This model is suitable for predicting GSM adsorption on PAC different surfaces, thus avoiding limiting the increased sorbate concentration generally associated with the Freundlich model. Therefore, at low adsorbate concentration, this model is reduced to the Freundlich model.

The Toth isotherm model is most useful in describing heterogeneous adsorption systems that meet both the low and high-end limits of the adsorbate concentration [64]. n is Toth isotherm constant (μg mg^{-1}) characterizes the heterogeneity of the adsorption system, then the sorptions of 2-MIB and GSM are said to be heterogeneous.

3.4.3. Mechanism

In this study, the Elovich, intraparticle diffusion, Modified intraparticle diffusion, liquid film diffusion, and Bangham models were utilized to acknowledge both the adsorption mechanism deeply for 2-MIB and GSM by PAC. We categorized the mechanism to find an adsorption mechanism pathway. The Elovich model was used to determine the chemical or physical adsorption. The intraparticle diffusion was utilized to investigate the limitation of diffusion was or not? The liquid film diffusion and Bangham models were used to examine the liquid to solid adsorption rate and pore diffusion activities such as multiple adsorption stages, respectively.

As a result of the kinetic model analysis performed with the adsorption dynamics data in terms of all ambient conditions and metabolites shown in Table 5, it was observed that a single model did not fully express all adsorption mechanisms. The most striking observation to emerge from the data analysis was good correlation and high R^2 values. Although it varies depending on the type of metabolite and experimental conditions, predominantly, the intraparticle diffusion model has well-expressed 2-MIB and GSM adsorption. Besides, it has been observed that other examined kinetic models can express the adsorption event from

Table 5
The kinetic parameters for adsorption mechanism models

Kinetics	Elovich	Intraparticle diffusion	Modified intraparticle diffusion	Liquid film diffusion	Bangham
2-MIB					
Parameters	$\alpha = 0.4284$	$C = 0.3717$	$\alpha = 0.2091$	$k_{FD} = 0.0324$	$\alpha = 0.3650$
	$\beta = 7.1557$	$k_{id} = 0.0453$	$k_{id} = 0.2915$		$k_0 = 0.0029$
R^2	0.9518	0.9864	0.9706	0.9789	0.9507
GSM					
Parameters	$\alpha = 1.2370$	$C = 0.4774$	$\alpha = 0.1682$	$k_{FD} = 0.0370$	$\alpha = 0.3197$
	$\beta = 8.0768$	$k_{id} = 0.0399$	$k_{id} = 0.3677$		$k_0 = 0.0040$
R^2	0.9623	0.9844	0.9698	0.9789	0.9600

a kinetic perspective. It can be said that only one kinetic model is insufficient in explaining the adsorption event due to the high initial pollutant concentrations in this study. At the same time, different mechanisms affect the development of adsorption at different intensities. The progress of possible adsorption occurred similarly because the 2-MIB and GSM metabolites have similar organic structures.

Our investigation showed that the value of the regression coefficient (R^2) for the Elovich model was 0.9518 and 0.9623, which is higher than that of Langmuir; therefore, the adsorption of 2-MIB and GSM onto PAC was best described by the Elovich isotherm. The equation that defines this model is based on a kinetic principle, which assumes that adsorption sites increase exponentially with adsorption; this implies multilayer adsorption [65].

According to the experimental data, the intraparticle diffusion model was best fitted than other mechanism models for both 2-MIB and GSM metabolites. It is stated that the intraparticle diffusion model curve shows more than one linear state and consists of two parts. External resistance, which impedes the mass transfer surrounding the particle, is considered to occur only in the initial stages of adsorption. This situation happened in the first part. The second linear part is a gradually increasing adsorption step where intraparticle diffusion is dominant. These parts can be defined as macro transport and meso/micropore diffusion, respectively. The first part is the area where the external surface adsorption takes place, and it takes about 16 min for both metabolites. In this part, physical adsorption occurred, and it was reversible. The molecules pass through the macropores. The second part shows the gradual adsorption state, and this part limited the intraparticle diffusion rate occurred. The second part, which occurred in about 74 min, was prolonged and this part was associated with the mesopores. In the last part, the third part, diffusion slows down and reaches equilibrium. Our study results showed that adsorption was finished in the second part (90 min) this situation was associated with the 2-MIB and GSM pores. These pollutants have mesopores, so they did not pass through the micropores, and the third part has not occurred. One unexpected finding was that the intraparticle diffusion model had positive *C*-values (2-MIB = 0.3717 and GSM = 0.4774) that can be seen in Table 5. The kinetic parameters for adsorption mechanism models. This shows this diffusion model is not only the factor affecting the adsorption process [66]. Greenwald et al. [67] developed a rapid kinetic dye test to predict the adsorption of 2-MIB onto granular steam activated carbons with different pore volumes and indicated that *C*-values were positive. Both kinetic and mechanism studies also reveal that both physical and chemical adsorption was occurred like in our study.

According to the liquid film diffusion kinetic model, the sorption rate of sorbates (k_{FD}) from the liquid phase to the solid phase was approximately 0.0350 min^{-1}, and the decisive step was film diffusion. Then, the Bangham model was used to investigate the adsorbate pore diffusion activities [68]. It can be said that multiple adsorption stages occurred during the adsorption. The high R^2 values of the Bangham model suggested that pore diffusion was involved in 2-MIB and GSM on PAC. The α values of the Bangham model should be lower than 1. Our experimental results also indicated that ◎ values were 0.3650 and 0.3197 for 2-MIB and GSM, as similar to the previous study [68]. The linearity of the Bangham plot also showed that not only pore diffusion occurred, but also multiple mechanisms also occurred.

4. Conclusions

In this laboratory-scale study, although 95% removal of 2-MIB and GSM components has been achieved with coconut-originated steam-activated carbon adsorption, it is unlikely to achieve this efficiency in applications in real treatment plants.

PAC was used for adsorption of GSM and MIB, which cause taste and odor problems in surface waters. PAC characterization preferred as sorbent has been determined by EN 12903 standard, and it has been found suitable for drinking water treatment. Also, the activation and surface structure of the sorbent was interpreted with SEM images. Adsorption experiments were performed by spiking 2-MIB and GSM on the raw drinking water samples varying at the mesotrophic and eutrophic levels, which were characterized in 12 months. Optimum conditions for approximately 100 μg L^{-1} GSM and MIB removal were determined as PAC = 100 mg L^{-1}, pH = 7.05, and t = 90 min.

Surprisingly, the kinetic study clearly shows that the film diffusion, surface sorption, and intraparticle diffusion mechanisms occurs together. These kinetic results help us to understand how physical and chemical adsorption

occurs unlimitedly. It seems likely that these results are in fact due to the BET isotherm results. According to the isotherms results, MIB adsorption was irreversible (due to the Langmuir isotherm) and adsorption was occurred regardless of temperature (Temkin and Dubinin–Radushkevich isotherms).

This study broadened the knowledge of using PAC to treat GSM and MIB in DWTPs and provided a basis for the giving an information to be used by operators of DWTPs to adjust operating conditions such as contact time, the concentration of metabolites, initial pH of the solution, and dosage of activated carbon. Moreover, this study set out to giving information about the activation, origin, and suitability of usability as an adsorbent in drinking water treatment plants of activated carbon.

Symbols and abbreviations

2-MIB	—	2-Methylisoborneol
GSM	—	Geosmin
PAC	—	Powdered activated carbon
WTP	—	Water treatment plant
US EPA	—	The United States Environmental Protection Agency
WHO	—	World Health Organization
NOM	—	Natural organic matter
GC/MS	—	Gas chromatography/Mass spectrometry
TON	—	Total odor number
PAH	—	Polyaromatic hydrocarbons
C_0	—	Initial adsorbate concentration, mg L^{-1}
C_e	—	Equilibrium liquid-phase concentration of the adsorbate, mg L^{-1}
m	—	Adsorbent dosage, g L^{-1}
q_e	—	Equilibrium adsorption capacity, mg g^{-1}
q_S	—	Theoretical saturation capacity, mg g^{-1}
q_{max}	—	Theoretical monolayer capacity, mg g^{-1}
k_0	—	Zero-order rate constant, mg g^{-1} min^{-1}
k_1	—	First-order rate constant, min^{-1}
k_2	—	Second-order rate constant, g mg^{-1} min^{-1}
k_B	—	Bhattacharya & Venchobacher rate constant
a	—	Exponential equality constant
b	—	Exponential equality constant
α	—	Initial adsorption rate; mg g^{-1} min^{-1}
β	—	Desorption constant, g mg^{-1}
k_{id}	—	Intraparticle diffusion rate constant, mg g^{-1} $min^{-1/2}$
R	—	Percentage of adsorbed substance, %
k_F	—	Freundlich isotherm constant related to the sorption capacity, L g^{-1}
$1/n$	—	Freundlich isotherm constant
k_L	—	Langmuir isotherm constant, L mg^{-1}
R_L	—	Dimensionless Langmuir equilibrium parameter, mg g^{-1}
k_T	—	Temkin isotherm equilibrium constant, L mg^{-1}
R	—	Universal gas constant, 0.008314 kJ mol^{-1} K^{-1}
T	—	Absolute temperature, °K
b_T	—	Temkin constant related to the heat of adsorption, J mol^{-1}
$q_{e,exp}$	—	Experimental concentration of adsorbate on the adsorbent
$q_{e,cal}$	—	Theoretical concentration of adsorbate on the adsorbent
k_{HE}	—	Henry's adsorption constant
θ	—	Degree of surface coverage
θ_F	—	Fractional coverage
w	—	Interaction energy of adsorbed molecules, kJ mol^{-1}
E	—	Mean free energy of adsorption
C_{BET}	—	Brunauer–Emmett–Teller isotherm constant
ε	—	Dubinin–Radushkevich isotherm constant
k_D	—	Dubinin–Radushkevich isotherm constant, mol^2 kJ^{-2}
A_{HJ}	—	Harkins–Jura adsorption constant
B_{HJ}	—	Harkins–Jura adsorption constant
k_H	—	Halsey isotherm constant
n_H	—	Halsey isotherm constant
k_{RP}	—	Redlich–Peterson isotherm constant, L g^{-1}
a_{RP}	—	Redlich–Peterson isotherm constant, L mg^{-1}
β	—	Redlich–Peterson exponent which lies between 0 and 1
b_S	—	Sips isotherm constant related to the energy of adsorption
k_T	—	Toth model adsorption isotherm constant
n_t	—	Toth model exponent
N	—	Number of experimental points
j	—	Number of data points
R^2	—	Coefficient of determination
SSE	—	Sum of squares errors
SAE	—	Sum of absolute errors
ARE	—	Average relative errors
HYBRID	—	The hybrid fractional error function
MPSD	—	Marquardt's percent standard deviation
χ^2	—	Non-linear chi-square test

Competing interest

The authors declare that they have no competing interests.

Consent for publication

Not applicable.

Ethics approval and consent to participate

Not applicable.

Funding

This work was not funded.

Availability of data and materials

The authors confirm that the data supporting the findings of this study are available within the article.

Authors' contributions

All authors designed and directed the research; Alver and Başтürk processed the experimental data, performed

the analysis, drafted the manuscript, and Alver and Işık applied to models. All authors aided in interpreting the results worked on the manuscript, and discussed the results, and commented on the manuscript.

Acknowledgments

I want to thank my colleagues at the Environmental Engineering Department of Aksaray University for their advice, comments, and help in other ways during this paper. Most of all, I would like to say something to my dear uncle, Dr. Fatih Sarpkaya, who passed away on February 9, 2022. "I cannot thank you enough for raising, loving, and supporting me, which forms the foundations of my life today. I will never forget you. The more of life I experience, the more I realize the depth of your wisdom. May your soul rest in peace."

References

[1] J. Huang, C.-c. Xu, B.G. Ridoutt, X.-c. Wang, P.-a. Ren, Nitrogen and phosphorus losses and eutrophication potential associated with fertilizer application to cropland in China, J. Cleaner Prod., 159 (2017) 171–179.
[2] M.M.G. Berlt, R. de Cassia de Souza Schneider, Ê.L. Machado, L.T. Kist, Comparative assessment of the degradation of 2-methylisoborneol and geosmin in freshwater using advanced oxidation processes, Environ. Technol., 42 (2021) 3832–3839.
[3] N. John, A.V. Koehler, B.R.E. Ansell, L. Baker, N.D. Crosbie, A.R. Jex, An improved method for PCR-based detection and routine monitoring of geosmin-producing cyanobacterial blooms, Water Res., 136 (2018) 34–40.
[4] R. Callejón, C. Ubeda, R. Ríos-Reina, M. Morales, A. Troncoso, Recent developments in the analysis of musty odor compounds in water and wine: a review, J. Chromatogr. A, 1428 (2016) 72–85.
[5] R.L. Bristow, I.S. Young, A. Pemberton, J. Williams, S. Maher, An extensive review of the extraction techniques and detection methods for the taste and odour compound geosmin (*trans*-1, 10-dimethyl-*trans*-9-decalol) in water, TrAC, Trends Anal. Chem., 110 (2019) 233–248.
[6] R. Srinivasan, G.A. Sorial, Treatment of taste and odor causing compounds 2-methyl isoborneol and geosmin in drinking water: a critical review, J. Environ. Sci., 23 (2011) 1–13.
[7] X. Li, P. Lin, J. Wang, Y. Liu, Y. Li, X. Zhang, C. Chen, Treatment technologies and mechanisms for three odorants at trace level: IPMP, IBMP, and TCA, Environ. Technol., 37 (2016) 308–315.
[8] G. Izaguirre, W.D. Taylor, A guide to geosmin- and MIB-producing cyanobacteria in the United States, Water Sci. Technol., 49 (2004) 19–24.
[9] S. Suurnäkki, G.V. Gomez-Saez, A. Rantala-Ylinen, J. Jokela, D.P. Fewer, K. Sivonen, Identification of geosmin and 2-methylisoborneol in cyanobacteria and molecular detection methods for the producers of these compounds, Water Res., 68 (2015) 56–66.
[10] N.N. Gerber, H.A. Lechevalier, Geosmin, an earthy-smelling substance isolated from actinomycetes, Appl. Environ. Microbiol., 13 (1965) 935–938.
[11] M. Su, J. Yu, J. Zhang, H. Chen, W. An, R.D. Vogt, T. Andersen, D. Jia, J. Wang, M. Yang, MIB-producing cyanobacteria (*Planktothrix* sp.) in a drinking water reservoir: distribution and odor producing potential, Water Res., 68 (2015) 444–453.
[12] A. Zamyadi, R. Henderson, R. Stuetz, R. Hofmann, L. Ho, G. Newcombe, Fate of geosmin and 2-methylisoborneol in full-scale water treatment plants, Water Res., 83 (2015) 171–183.
[13] W. Schmidt, H. Petzoldt, K. Bornmann, L. Imhof, C. Moldaenke, Use of cyanopigment determination as an indicator of cyano-toxins in drinking water, Water Sci. Technol., 59 (2009) 1531–1540.
[14] T.-F. Lin, S. Watson, A.M. Dietrich; I.H. (Mel) Suffet, Taste and Odour in Source and Drinking Water: Causes, Controls, and Consequences, IWA Publishing, UK, 2018.
[15] M. Fakıoğlu, M.E. Karpuzcu, İ. Toröz, F. Yıldız, İ. Öztürk, İçme sularından tat ve kokunun giderimi: İstanbul'daki kurulu su arıtma tesislerinde performans değerlendirmesi ve iyileştirilmesi, Removal of taste and odor from drinking water: performance evaluation and upgrade options for the treatment plants in Istanbul, Pamukkale Univ. J. Eng. Sci., 26 (2019) 505–512, doi: 10.5505/pajes.2019.78949.
[16] L. Ho, P. Tanis-Plant, N. Kayal, N. Slyman, G. Newcombe, Optimising water treatment practices for the removal of *Anabaena circinalis* and its associated metabolites, geosmin and saxitoxins, J. Water Health, 7 (2009) 544–556.
[17] Q. Wang, F. Zietzschmann, J. Yu, R. Hofman-Caris, W. An, M. Yang, L.C. Rietveld, Projecting competition between 2-methylisoborneol and natural organic matter in adsorption onto activated carbon from ozonated source waters, Water Res., 173 (2020) 115574, doi: 10.1016/j.watres.2020.115574.
[18] R. Nerenberg, B.E. Rittmann, W.J. Soucie, Ozone/biofiltration for removing MIB and geosmin, J. Am. Water Works Assn., 92 (2000) 85–95.
[19] K. Doederer, D. Gale, J. Keller, Effective removal of MIB and geosmin using MBBR for drinking water treatment, Water Res., 149 (2019) 440–447.
[20] C. Directive, Council Directive 67/548/EEC of 27 June 1967 on the Approximation of Laws, Regulations and Administrative Provisions Relating to the Classification, Packaging and Labelling of Dangerous Substances, OJEC, 196 (1967) 1.
[21] E. Bertone, C. Chang, P. Thiel, K. O'Halloran, Analysis and modelling of powdered activated carbon dosing for taste and odour removal, Water Res., 139 (2018) 321–328.
[22] Shimadzu, Analysis of Musty Odors using SPME-GC/MS, Shimadzu Application News, Tokyo, 2020.
[23] Z. Harrache, M. Abbas, T. Aksil, M. Trari, Thermodynamic and kinetics studies on adsorption of Indigo Carmine from aqueous solution by activated carbon, Microchem. J., 144 (2019) 180–189.
[24] N.S. Yousef, R. Farouq, R. Hazzaa, Adsorption kinetics and isotherms for the removal of nickel ions from aqueous solutions by an ion-exchange resin: application of two and three parameter isotherm models, Desal. Water Treat., 57 (2016) 21925–21938.
[25] A. Berkem, S. Baykut, M. Berkem, Fizikokimya İkinci Cilt, İstanbul Üniversitesi Yayınları, 1994.
[26] N. Ayawei, A.N. Ebelegi, D. Wankasi, Modelling and interpretation of adsorption isotherms, J. Chem., 2017 (2017) 3039817, doi: 10.1155/2017/3039817.
[27] W. Taylor, R. Losee, M. Torobin, G. Izaguirre, D. Sass, D. Khiari, K. Atasi, Early Warning and Management of Surface Water Taste-and-Odor Events, American Water Works Association (AWWA), Denver, CO, USA, 2006.
[28] A. Kurnaz, E. Mutlu, A.A. Uncumusaoğlu, Determination of water quality parameters and heavy metal content in surface water of Çiğdem Pond (Kastamonu/Turkey), Turkish J. Agric. – Food Sci. Technol., 4 (2016) 907–913.
[29] M. Fakıoğlu, M.E. Karpuzcu, İ. Öztürk, İçme sularında alg kaynaklı tat ve koku sorununun değerlendirilmesi, PAJES, 24 (2018).
[30] C. Ng, J.N. Losso, W.E. Marshall, R.M. Rao, Freundlich adsorption isotherms of agricultural by-product-based powdered activated carbons in a geosmin–water system, Bioresour. Technol., 85 (2002) 131–135.
[31] M. Işık, Ötrofikasyon ve Su Kalitesi Problemleri-Aksaray Örneği, İklim Değişikliği ve Çevre, 3 (2018) 37–44.
[32] S. Sabater, E. Vilalta, A. Gaudes, H. Guasch, I. Muñoz, A. Romaní, Ecological implications of mass growth of benthic cyanobacteria in rivers, Aquat. Microb. Ecol., 32 (2003) 175–184.
[33] S.B. Watson, Aquatic taste and odor: a primary signal of drinking-water integrity, J. Toxicol. Environ. Health Part A, 67 (2004) 1779–1795.
[34] J.A. Downing, S.B. Watson, E. McCauley, Predicting cyanobacteria dominance in lakes, Can. J. Fish. Aquat. Sci., 58 (2001) 1905–1908.
[35] B.S.P.a.S. Committee, BS EN 12903:2009, Products Used for the Treatment of Water Intended for Human Consumption: Powdered Activated Carbon, UK, 2009.

[36] M. Danish, T. Ahmad, A review on utilization of wood biomass as a sustainable precursor for activated carbon production and application, Renewable Sustainable Energy Rev., 87 (2018) 1–21.
[37] M. Mitchek, Functional Impact of Natural Organic Matter on the Adsorption of 2-Methylisoborneol and Geosmin to Powdered Activated Carbon, Colorado School of Mines, 2021.
[38] L. Qiang, W. Qunshan, H. Xin, Y. Kai, W. Yang, T. Lipeng, J. Zeyu, Y. Jianwei, S. Baoyou, Powdered activated carbon for treatment of musty odor in a Southern China water treatment plant, Chin. J. Environ. Eng., 12 (2018) 3034–3042.
[39] E.Y. Küçükgül, Ticari aktif karbon üretimi ve özelliklerinin belirlenmesi, 2004.
[40] H. Marsh, Activated Carbon Compendium: A Collection of Papers from the Journal Carbon 1996–2000, Elsevier Science Ltd., UK, 2001.
[41] I. Morgan, C. Fink, Activated carbon production, Chem. Ind. Eng., 2 (1989) 219.
[42] O. Kadlec, The Characterization of Porous Solids, Proceeding Swiss-British Symp. SCI, London, 1979.
[43] B.D. Zdravkov, J.J. Čermák, M. Šefara, J. Janků, Pore classification in the characterization of porous materials: a perspective, Open Chem. J., 5 (2007) 385–395.
[44] M.S. Shafeeyan, W.M.A.W. Daud, A. Houshmand, A. Shamiri, A review on surface modification of activated carbon for carbon dioxide adsorption, J. Anal. Appl. Pyrolysis, 89 (2010) 143–151.
[45] H. Jankowska, A. Świątkowski, J. Choma, Active Carbon, Ellis Horwood Ltd., UK, 1991.
[46] Y. Kuang, X. Zhang, S. Zhou, Adsorption of methylene blue in water onto activated carbon by surfactant modification, Water, 12 (2020) 587, doi: 10.3390/w12020587.
[47] X. Wang, N. Zhu, B. Yin, Preparation of sludge-based activated carbon and its application in dye wastewater treatment, J. Hazard. Mater., 153 (2008) 22–27.
[48] N. Kannan, M.M. Sundaram, Kinetics and mechanism of removal of methylene blue by adsorption on various carbons—a comparative study, Dyes Pigm., 51 (2001) 25–40.
[49] Y. Chun, G. Sheng, C.T. Chiou, B. Xing, Compositions and sorptive properties of crop residue-derived chars, Environ. Sci. Technol., 38 (2004) 4649–4655.
[50] M. He, C. Chang, N. Peng, L. Zhang, Structure and properties of hydroxyapatite/cellulose nanocomposite films, Carbohydr. Polym., 87 (2012) 2512–2518.
[51] S. Hokkanen, A. Bhatnagar, A. Koistinen, T. Kangas, U. Lassi, M. Sillanpää, Comparison of adsorption equilibrium models and error functions for the study of sulfate removal by calcium hydroxyapatite microfibrillated cellulose composite, Environ. Technol., 39 (2018) 952–966.
[52] Y.-S. Ho, G. McKay, Pseudo-second-order model for sorption processes, Process Biochem., 34 (1999) 451–465.
[53] L. Ma, F. Peng, H. Li, C. Wang, Z. Yang, Adsorption of geosmin and 2-methylisoborneol onto granular activated carbon in water: isotherms, thermodynamics, kinetics, and influencing factors, Water Sci. Technol., 80 (2019) 644–653.
[54] A. Deb, M. Kanmani, A. Debnath, K.L. Bhowmik, B. Saha, Ultrasonic assisted enhanced adsorption of methyl orange dye onto polyaniline impregnated zinc oxide nanoparticles: kinetic, isotherm and optimization of process parameters, Ultrason. Sonochem., 54 (2019) 290–301.
[55] M. Belhachemi, F. Addoun, Comparative adsorption isotherms and modeling of methylene blue onto activated carbons, Appl. Water Sci., 1 (2011) 111–117.
[56] K. Ranganathan, Chromium removal by activated carbons prepared from *Casurina equisetifolia* leaves, J. Bioresour. Technol., 73 (2000) 99–103.
[57] D. Mohan, K.P. Singh, V.K. Singh, Removal of hexavalent chromium from aqueous solution using low-cost activated carbons derived from agricultural waste materials and activated carbon fabric cloth, Ind. Eng. Chem. Res., 44 (2005) 1027–1042.
[58] I. Tan, B. Hameed, A. Ahmad, Equilibrium and kinetic studies on basic dye adsorption by oil palm fibre activated carbon, Chem. Eng. J., 127 (2007) 111–119.
[59] C. Song, S. Wu, M. Cheng, P. Tao, M. Shao, G. Gao, Adsorption studies of coconut shell carbons prepared by KOH activation for removal of lead(II) from aqueous solutions, Sustainability, 6 (2014) 86–98.
[60] P.C. Hiemenz, R. Rajagopalan, Principles of Colloid and Surface Chemistry, Revised and Expanded, CRC Press, USA, 2016.
[61] S. Lowell, J.E. Shields, Powder Surface Area and Porosity, SSBM, China, 2013.
[62] K.Y. Foo, B.H. Hameed, Insights into the modeling of adsorption isotherm systems, Chem. Eng. J., 156 (2010) 2–10.
[63] G.P. Jeppu, T.P. Clement, A modified Langmuir–Freundlich isotherm model for simulating pH-dependent adsorption effects, J. Contam. Hydrol., 129 (2012) 46–53.
[64] T. Jafari Behbahani, Z. Jafari Behbahani, A new study on asphaltene adsorption in porous media, Pet. Coal, 56 (2014) 459–466.
[65] M. Gubernak, W. Zapala, K. Kaczmarski, Analysis of amylbenzene adsorption equilibria on an RP-18e chromatographic column, Acta Chromatogr., 13 (2003) 38–59.
[66] P. Wadhera, R. Jindal, R. Dogra, Synthesis of semi interpenetrating network hydrogel [(GrA-Psy)-cl-Poly (AA)] and its application for efficient removal of malachite green from aqueous solution, Polym. Eng. Sci., 59 (2019) 1416–1427.
[67] M.J. Greenwald, A.M. Redding, F.S. Cannon, A rapid kinetic dye test to predict the adsorption of 2-methylisoborneol onto granular activated carbons and to identify the influence of pore volume distributions, Water Res., 68 (2015) 784–792.
[68] A.A. Inyinbor, F.A. Adekola, G.A. Olatunji, Kinetics, isotherms and thermodynamic modeling of liquid phase adsorption of Rhodamine B dye onto *Raphia hookerie* fruit epicarp, Water Resour. Ind., 15 (2016) 14–27.

Supplementary information

Table S1
Analytical conditions and details of the detected 2-MIB and GSM

Autosampler	Shimadzu AOC-20i, Shimadzu Corporation, Japan.				
Instrument	Shimadzu GCMS-QP2010 Plus				
GC column	Rxi-624Sil MS, 60.00 m, 0.25 mm ID, 1.40 μm (Restek, Germany)				
GC					
Injection temp.	200°C				
Column temp.	35°C (hold 1 min) to 225°C@30°C/min (hold 11 min)				
Carrier gas	Helium, constant flow@1.40 mL min^{-1}				
Injection method	Splitless				
MS					
Interface temp.	225°C				
Ion source temp.	200°C				
Monitor ion	2-MIB: 95, 107, 43 Geosmin: 112, 41, 55				
Compound	t_R (min)	T_{peak} (°C)	R^2	LOQ (μg L^{-1})	Reproducibility CV (%)
2-Methylisoborneol	12.38	225	0.9996	1.422	3.334
Geosmin	16.99	225	0.9967	1.036	3.002

Table S2
List of adsorption models

Model	Non-linear form	Linear form	Plot	Slope and intercept
Kinetics				
Pseudo-first-order	$q_t = q_e\left(1-e^{-k_1 t}\right)$	$\ln\left(q_e - q_t\right) = \ln q_e - k_1 t$	$\ln\left(q_e - q_t\right)$ vs t	Slope : $-k_1$, Intercept : $\ln q_e$
Pseudo-second-order	$q_t = \frac{q_e^2 k_2 t}{1+q_e k_2 t}$	$\frac{t}{q_t} = \frac{1}{k_2 q_e^2} + \frac{t}{q_e}$	$\frac{t}{q_t}$ vs t	Slope : $\frac{1}{q_e}$, Intercept : $\frac{1}{k_2 q_e^2}$
Bhattacharya & Venchobacher		$\ln\left(1-U_t\right) = k_b t$ $U_t = \frac{C_0 - C_t}{C_0 - C_e}$	$\ln\left(1-U_t\right)$ vs t	Slope : k_b, Intercept : –
Elovich	$q_t = \beta \ln\left(\alpha\beta t\right)$	$q_t = \frac{1}{\beta}\ln\left(\alpha\beta\right) + \frac{1}{\beta}\ln t$	q_t vs $\ln t$	Slope : $\frac{1}{\beta}$, Intercept : $\frac{1}{\beta}\ln\left(\alpha\beta\right)$
Intraparticle diffusion		$q_t = k_{\mathrm{id}} t^{1/2} + a$	q_t vs $t^{1/2}$	Slope : k_{id}, Intercept : a
Liquid film diffusion		$\ln\left(1-\frac{q_t}{q_e}\right) = -0.4977 - k_{\mathrm{FD}} t$	$\ln\left(1-\frac{q_t}{q_e}\right)$ vs t	Slope : $-k_{\mathrm{FD}}$, Intercept : -0.4977
Bangham		$\log\log\left(\frac{C_0}{C_0 - q_t m}\right) = \log\left(\frac{k_0 t}{2.303V}\right) + a\log t$	$\log\log\left(\frac{C_0}{C_0 - q_t m}\right)$ vs $\log t$	Slope : a, Intercept : $\log\left(\frac{k_0 t}{2.303V}\right)$
Two-parameter isotherms				
Freundlich	$q_e = k_F C_e^{1/n}$	$\log\left(q_e\right) = \log\left(k_F\right) + \frac{1}{n}\log\left(C_e\right)$	$\log\left(q_e\right)$ vs $\log\left(C_e\right)$	Slope : $\frac{1}{n}$, Intercept : $\log\left(k_F\right)$
Langmuir	$q_e = \frac{q_{\max} k_L C_e}{1+k_L C_e}$	$\frac{C_e}{q_e} = \frac{1}{q_{\max} k_L} + \frac{C_e}{q_{\max}}$ $R_L = \frac{1}{1+q_{\max} k_L}$	$\frac{C_e}{q_e}$ vs C_e	Slope : $\frac{1}{q_{\max}}$, Intercept : $\frac{1}{k_L q_{\max}}$
Temkin	$q_e = \frac{RT}{b_T}\ln\left(k_T C_e\right)$	$q_e = \frac{RT}{b_T}\ln\left(k_T\right) + \frac{RT}{b_T}\ln\left(C_e\right)$	q_e vs $\ln\left(C_e\right)$	Slope : $\frac{RT}{b_T}$, Intercept : $\frac{RT}{b_T}\ln\left(k_T\right)$

Table S2 *Continued*

Model	Non-linear form	Linear form	Plot	Slope and intercept
Dubinin–Radushkevich	$q_e = q_s e^{-k_D \varepsilon^2}$	$\ln q_e = \ln q_s - k_D \varepsilon^2$ $\varepsilon = RT \ln\left(1 + \frac{1}{C_e}\right)$ $E = \frac{1}{\sqrt{2k_D}}$	$\ln q_e$ vs ε^2	Slope : $-k_D$, Intercept : $\ln q_s$
Brunauer–Emmett–Teller	$q_e = \frac{q_s C_{\text{BET}} C_e}{\left(C_s - C_e\right)\left[1 + \left(C_{\text{BET}} - 1\right)\left(C_e / C_s\right)\right]}$	$\frac{C_e}{q_e\left(C_s - C_e\right)} = \frac{1}{q_s C_{\text{BET}}} + \frac{\left(C_{\text{BET}} - 1\right)}{q_g C_{\text{BET}}} \frac{C_e}{C_s}$	$\frac{C_e}{q_e\left(C_S - C_e\right)}$ vs $\frac{C_e}{C_s}$	Slope : $\frac{\left(C_{\text{BET}} - 1\right)}{q_s C_{\text{BET}}}$, Intercept : $\frac{1}{q_s C_{\text{BET}}}$
Harkins–Jura	$q_e = \left(\frac{A_{\text{HJ}}}{B_{\text{HI}} - \log C_e}\right)^{\frac{1}{2}}$	$\frac{1}{q_e^2} = \frac{B_{\text{HJ}}}{A_{\text{HI}}} - \left(\frac{1}{A_{\text{HI}}}\right) \log C_e$	$\frac{1}{q_e^2}$ vs $\log C_e$	Slope : $-\left(\frac{1}{A_{\text{HI}}}\right)$, Intercept : $\frac{B_{\text{HJ}}}{A_{\text{HI}}}$
Halsey	$q_e = e^{\left(\frac{\ln k_H - \ln C_e}{n_H}\right)}$	$\ln\left(q_e\right) = \frac{1}{n_H} \ln\left(k_H\right) - \frac{1}{n_H} \ln\left(C_e\right)$	$\ln\left(q_e\right)$ vs $\ln\left(C_e\right)$	Slope : $-\frac{1}{n_H}$, Intercept : $\frac{1}{n_H} \ln\left(k_H\right)$
Three-parameter isotherms				
Redlich–Peterson	$q_e = \frac{k_R C_e}{1 + a_R C_e^{\alpha}}$	$\ln\left(k_R \frac{C_e}{q_e} - 1\right) = \alpha \ln\left(C_e\right) + \ln\left(a_R\right)$	$\ln\left(k_R \frac{C_e}{q_e} - 1\right)$ vs $\ln\left(C_e\right)$	Slope : α, Intercept : $\ln\left(a_R\right)$
Sips	$q_e = \frac{q_m k_s C_e^{1/n}}{1 + k_s C_e^{1/n}}$	$\ln\left(\frac{q_e}{q_m - q_e}\right) = \frac{1}{n} \ln\left(C_e\right) + \ln\left(k_s\right)^{\frac{1}{n}}$	$\ln\left(\frac{q_e}{q_m - q_e}\right)$ vs $\ln\left(C_e\right)$	Slope : $\frac{1}{n}$, Intercept : $\ln\left(k_s\right)^{\frac{1}{n}}$
Toth	$q_e = \frac{k_T C_e}{\left(a_T C_e\right)^{1/t}}$	$\ln\left(\frac{q_e^{n_t}}{q_m^{n_t} - q_e^{n_t}}\right) = n_t \ln\left(C_e\right) + n_t \ln\left(k_T\right)$	$\ln\left(\frac{q_e^{n_t}}{q_m^{n_t} - q_e^{n_t}}\right)$ vs $\ln\left(C_e\right)$	Slope : n_t, Intercept : $n_t \ln\left(k_T\right)$

Table S3
Expression of different error functions [26]

Error function	Abbreviation	Expression
Coefficient of determination	R^2	$\frac{\sum\left(q_{e,\exp}-q_{e,\mathrm{cal}}\right)^2}{\sum\left(q_{e,\exp}-q_{e,\mathrm{cal}}\right)^2+\left(q_{e,\exp}-q_{e,\mathrm{cal}}\right)^2}$
Sum of squares errors	SSE or ERRSQ	$\sum_{i=1}^{j}\left(q_{e,\exp}-q_{e,\mathrm{cal}}\right)_i^2$
Sum of absolute errors	SAE or EABS	$\sum_{i=1}^{j}\left\lvert q_{e,\exp}-q_{e,\mathrm{cal}}\right\rvert_i^2$
Average relative errors	ARE	$\frac{100}{j}\sum_{i=1}^{j}\left\lvert\frac{q_{e,\exp}-q_{e,\mathrm{cal}}}{q_{e,\exp}}\right\rvert_i$
A hybrid fractional error function	HYBRID	$\frac{100}{j-p}\sum_{i=1}^{j}\left\lvert\frac{q_{e,\exp}-q_{e,\mathrm{cal}}}{q_{e,\exp}}\right\rvert_i$
Marquardt's percent standard deviation	MPSD	$\sqrt[100]{\frac{1}{j-p}\sum_{i=1}^{j}\left(\frac{q_{e,\exp}-q_{e,\mathrm{cal}}}{q_{e,\exp}}\right)_i}$
Non-linear chi-square test	χ^2	$\sum_{i=1}^{j}\frac{\left(q_{e,\mathrm{cal}}-q_{e,\exp}\right)_i^2}{q_{e,\exp}}$